Nanoscale Magnetization Reversal Caused by Electric Field-Induced Ion Migration and Redistribution in Cobalt Ferrite Thin Films

Xinxin Chen,[†,⊥,#] Xiaojian Zhu,[†,⊥,#] Wen Xiao,[‡] Gang Liu,[*,†,⊥] Yuan Ping Feng,[§] Jun Ding,[*,†,‡,⊥] and Run-Wei Li[*,†,⊥]

[†]Key Laboratory of Magnetic Materials and Devices and [⊥]Zhejiang Province Key Laboratory of Magnetic Materials and Application Technology, Ningbo Institute of Materials Technology and Engineering, Chinese Academy of Sciences, Ningbo, Zhejiang 315201, China, [‡]Department of Materials Science and Engineering, National University of Singapore, 119260, Singapore, and [§]Department of Physics, National University of Singapore, 117542, Singapore. [#]X. Chen and X. Zhu contributed equally to this work.

ABSTRACT Reversible nanoscale magnetization reversal controlled merely by electric fields is still challenging at the moment. In this report, first-principles calculation indicates that electric field-induced magnetization reversal can be achieved by the appearance of unidirectional magnetic anisotropy along the (110) direction in Fe-deficient cobalt ferrite ($CoFe_{2-x}O_4$, CFO), as a result of the migration and local redistribution of the Co^{2+} ions adjacent to the B-site Fe vacancies. In good agreement with the theoretical model, we experimentally observed that in the CFO thin films the nanoscale magnetization can be reversibly and nonvolatilely reversed at room temperature *via* an electrical ion-manipulation approach, wherein the application of electric fields with appropriate polarity and amplitude can modulate the size of magnetic domains with different magnetizations up to 70%. With the low power consumption (subpicojoule) characteristics and the elimination of external magnetic field, the observed electric field-induced magnetization reversal can be used for the construction of energy-efficient spintronic devices, *e.g.*, low-power electric-write and magnetic-read memories.

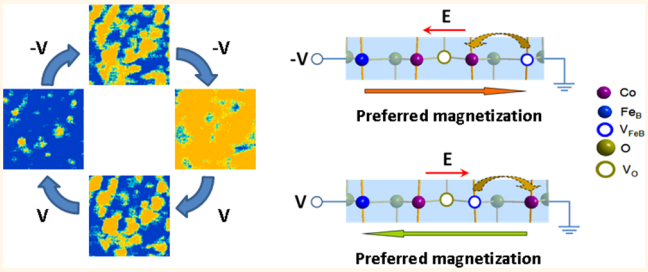

KEYWORDS: electric field control of magnetism · reversible magnetization reversal · ion migration and redistribution · cobalt ferrite thin films

Reversibly controlling the nanoscale magnetization at room temperature by electrical means would enable the development of various spintronic devices, in particular, novel magnetic information storage devices.[1−5] Although several approaches have been developed so far to achieve electrical modulation of magnetization reversal, most of these methods suffer from practical issues that hinder them from direct applications. For instance, the spin-torque effect, which is able to switch the magnetization of the magnetic domains by the interaction between a magnetic medium and the spin-polarized electric current flowing through it, usually faces the problem of high power consumption.[2,6] In the heterostructures wherein the magnetization could be regulated by an external electric field through the modulation of ferroelectric/ferromagnetic coupling *via* interfacial strain and/or charges, and exchange bias, as well as through the modulation of charge carrier concentration, the orbital occupation of 3*d* electrons, *etc.*, external magnetic fields are usually required.[7−15] Despite that other strategies have been reported to eliminate the need of a magnetic field for the realization of electric field control of magnetization recently, additional requirements of a low working temperature and complex sample structures may arise instead.[16−19] In view of these, more efforts should be devoted to designing novel device concepts wherein the reversal of magnetization can be achieved in a simple sample structure by solo electrical means and with low power consumption characteristics at room temperature.

* Address correspondence to runweili@nimte.ac.cn, liug@nimte.ac.cn, msedingj@nus.edu.sg.

Received for review January 21, 2015 and accepted March 20, 2015.

Published online March 20, 2015
10.1021/acsnano.5b00456

The nanoscale ion migration approach provides alternative possibilities for modulating the physical properties of semiconducting materials.[20−29] Very recently, it was reported that both cationic and anionic species can be manipulated to modulate the magnetic moment and/or magnetic anisotropy of magnetic oxides.[27,28] Cobalt ferrite ($CoFe_2O_4$), which is extensively used as magnetic recording media or used in electromagnetic and spintronic devices,[30,31] is another promising candidate for the realization of electric field control of magnetization *via* ion manipulation. Having an inverse spinel structure (AB_2O_4), all of the Co^{2+} cations and half of the Fe^{3+} cations occupy the octahedral sites (referred to B sites) in $CoFe_2O_4$, while the remaining Fe^{3+} cations stay at the tetrahedral sites (referred to A sites). The B-site Co^{2+} ion pairs and Fe^{3+} ion pairs are arranged alternatively along the ⟨110⟩ directions,[32] and Co^{2+} ions are responsible for the magnetic anisotropy of the material.[33] The cations also have the tendency to migrate through cation vacancies, which can be driven by annealing under magnetic field to induce the appearance of uniaxial magnetic anisotropy.[34−38] Comparatively, it is expected that the external electric fields may also provide the driving force for nanoscale ion migration[39−41] and consequently modulate the magnetization of $CoFe_2O_4$ thin films with cationic vacancies.

In this work, we theoretically propose that electric field-induced migration and local redistribution of the Co^{2+} ions adjacent to the B-site Fe^{3+} vacancies are capable of inducing unidirectional magnetic anisotropy in the (110)-textured $CoFe_{2-x}O_4$ (CFO) thin films with Fe vacancies.[42] Consequently, it is observed that nanoscale magnetization reversal can be achieved in a simple sandwich structure at room temperature *via* electrical ion-manipulation with low power consumption characteristics. The electrical modulation of magnetization in the CFO thin films is reversible and nonvolatile in nature and can be further assisted by the presence of oxygen vacancies. Without the assistance of an external magnetic field, the present strategy of utilizing electric field-induced migration and redistribution of ionic species to modulate the nanoscale magnetization at room temperature is considered more favorable for the construction of novel spintronic devices.

RESULTS AND DISCUSSION

In order to check the possibility of electrical modulation of magnetization reversal through the ion-manipulation approach, first-principles calculations were performed to investigate the correlation between the electric field-induced ion migration and redistribution and the magnetic anisotropy of CFO unit cells. As shown in Figure 1a, the B-site-paired Co^{2+} and Fe^{3+} ions are alternatively arranged along the ⟨110⟩ direction in an ideal $CoFe_2O_4$ unit cell. However, vacancies usually exist in the physically fabricated oxide thin films, wherein the nonstoichiometry may arise from the nonuniform distribution of the ionic species in the plasma glow or the scattering of the ions by the residue gas molecules. Calculation results show that the formation energy of the B-site Fe vacancies is lower than that of both the Co vacancies and the A-site Fe vacancies (Figure 1b). Therefore, the B-site Fe vacancies can be more easily formed in the CFO thin films. Nevertheless, the Fe vacancy prefers to stay between the two Co^{2+} ions with the lowest energy of this arrangement (Figure 1c). In the case that one Fe^{3+} ion is missing in the CFO unit cell and generates a B-site vacancy, when the electric field is applied along the $[\bar{1}\bar{1}0]$ direction, the second Co^{2+} ion will further migrate to take the middle cationic vacancy (Figure 1d). The back-diffusion energy barrier of this Co^{2+} cation is ~0.6 eV, which is sufficient to overcome the thermal disturbance at room temperature and make the system stable. In this circumstance, the redistribution of the Co^{2+} cation and the cationic vacancy breaks the symmetry of the unit cell, and the total energy of the unit cell with its magnetization pointing along the [110] direction is 1 meV smaller than that with the magnetization pointing in the opposite direction. This calculated unidirectional magnetic anisotropy energy difference (1 meV) is comparable to the magneto-crystalline anisotropy energy of the $CoFe_2O_4$ unit cell, by taking the magneto-crystalline anisotropy energy to be $\sim 1 \times 10^6$ J/m.[33,43] Consequently, the magnetization energetically prefers to point along [110] direction after the diffusion of Co^{2+} ions. When the external electric field is applied along the [110] direction, the Co^{2+} ion will drift back to its original position (Figure 1e), and the total energy of the unit cell with the magnetization pointing along the $[\bar{1}\bar{1}0]$ direction is 2 meV smaller than that with the magnetization pointing along the [110] direction. In this case, the preferred magnetization is aligned along the $[\bar{1}\bar{1}0]$ direction. Therefore, it is reasonable that the electric field-induced migration and local redistribution of Co^{2+} ions can result in the room-temperature magnetization reversal of the Fe-deficient CFO unit cell and thin film along the ⟨110⟩ directions.

Aiming to experimentally investigate the effect of external electric fields on the magnetization reversal, a 100 nm thick $SrRuO_3$ (SRO) thin film was first prepared onto the (110)-orientated $SrTiO_3$ (STO) single-crystal substrate by the pulsed laser deposition (PLD) technique to receive the conducting oxide electrode (see Methods). Then the (110)-textured CFO thin film with a thickness of 30 nm was deposited by the PLD technique on the SRO/STO structure at an oxygen pressure of 0.1 Pa (Figure 2a and b). Generally, $CoFe_2O_4$ is an inverse spinel ferrite with a cubic *Fm*3*m* structure, while both $SrRuO_3$ and $SrTiO_3$ also have cubic structures, therefore rendering that (110) textured

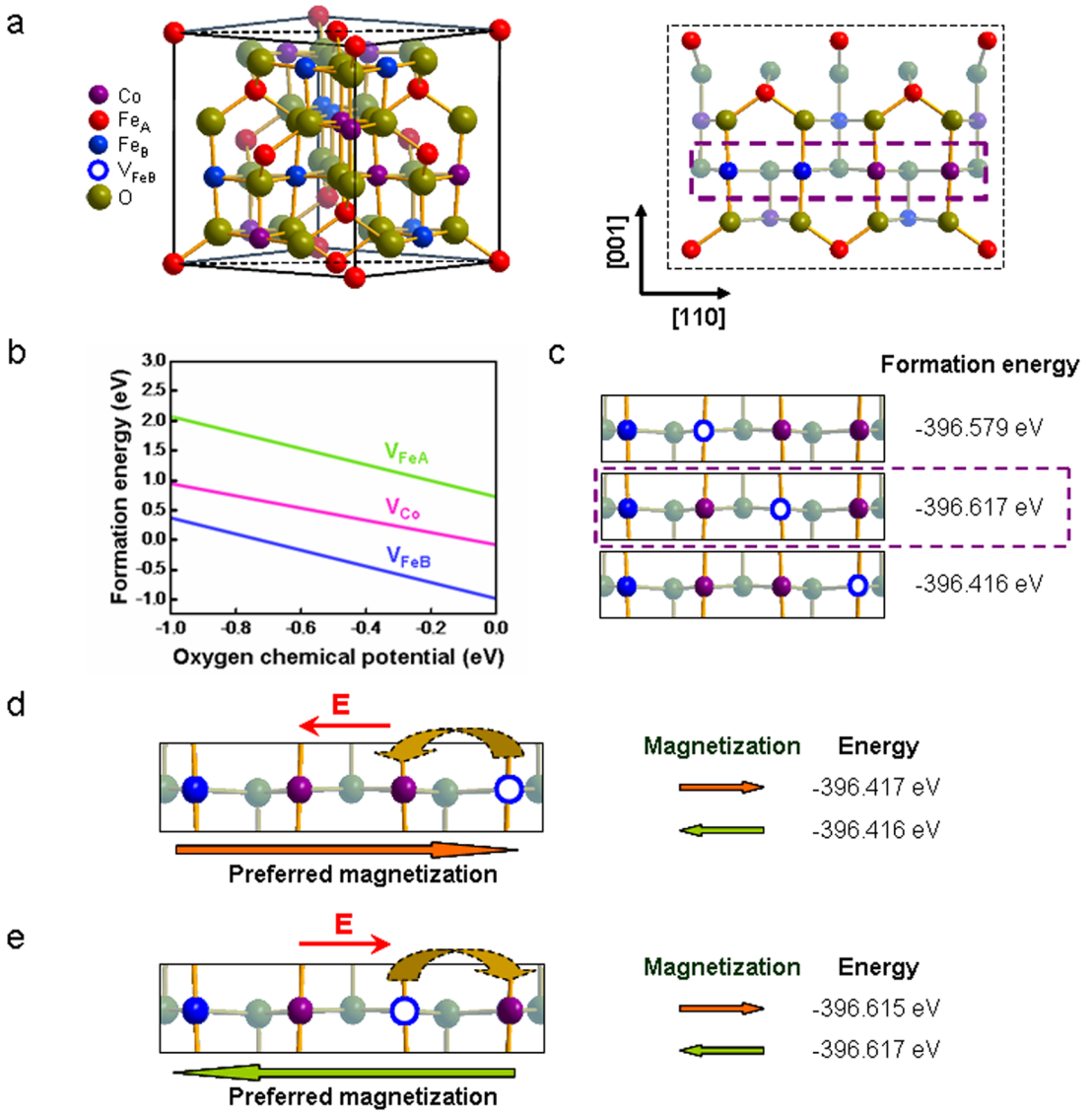

Figure 1. Theoretical model for the electric field-induced magnetization reversal in a CFO unit cell. (a) Lattice structure of an ideal $CoFe_2O_4$ unit cell (left panel) and the corresponding (110) plane (right panel). The dashed box marks the distribution of the cations along the [110] direction. (b) Dependence of the formation energy of the Co vacancy, A-site Fe vacancy, and B-site Fe vacancy on the oxygen chemical potential. (c) Localized structures of the CFO unit cell with different locations of the Fe vacancy occupation. (d, e) Localized structures and preferred magnetizations of the CFO unit cell with a Fe vacancy present along the [110] direction and with different locations of the Co^{2+} occupation after the occurrence of electric field-induced migration of Co^{2+} ions.

$CoFe_2O_4$ film can be deposited on the (110)-oriented $SrRuO_3/SrTiO_3$.[44] Although the (110) peak of the present CFO thin film was not observed due to the systematic extinction effect of X-ray diffraction, the presence of the (220) and (440) peaks observed at 2θ values of 30.2° and 62.6°, respectively, nevertheless confirms that (110) textured $CoFe_2O_4$ films were fabricated in the present study. The energy-dispersive X-ray (EDX) spectrum (Figure 2c) indicates that the as-fabricated CFO thin film has a Fe/Co atomic ratio of around 1.9, which is in good agreement with the crystal model for first-principles calculation where one Fe^{3+} ion is missing in a unit cell. Upon being annealed at 400 °C under a magnetic field of ~2000 Oe perpendicular to the film surface in a pure N_2 atmosphere for 10 h, the samples show out-of-plane uniaxial magnetic anisotropy, with the easy axis aligning along the [110] direction (Figure 2d).[37]

Then the Pt/Ir-coated conductive tip of the scanning probe microscope (SPM) was used as the counter electrode to construct the conductive tip/CFO/SRO sandwich structure and to load the electric field onto the CFO samples in the conductive atomic force microscopy (C-AFM) mode (Figure 3a). During the C-AFM operation, the conductive tip was always grounded and the biased voltage was applied on the SRO electrode. After removing the applied bias voltage, the magnetic domain structures of the same area were characterized using a Co/Cr-coated magnetic tip in the magnetic force microscopy (MFM) mode. As shown in

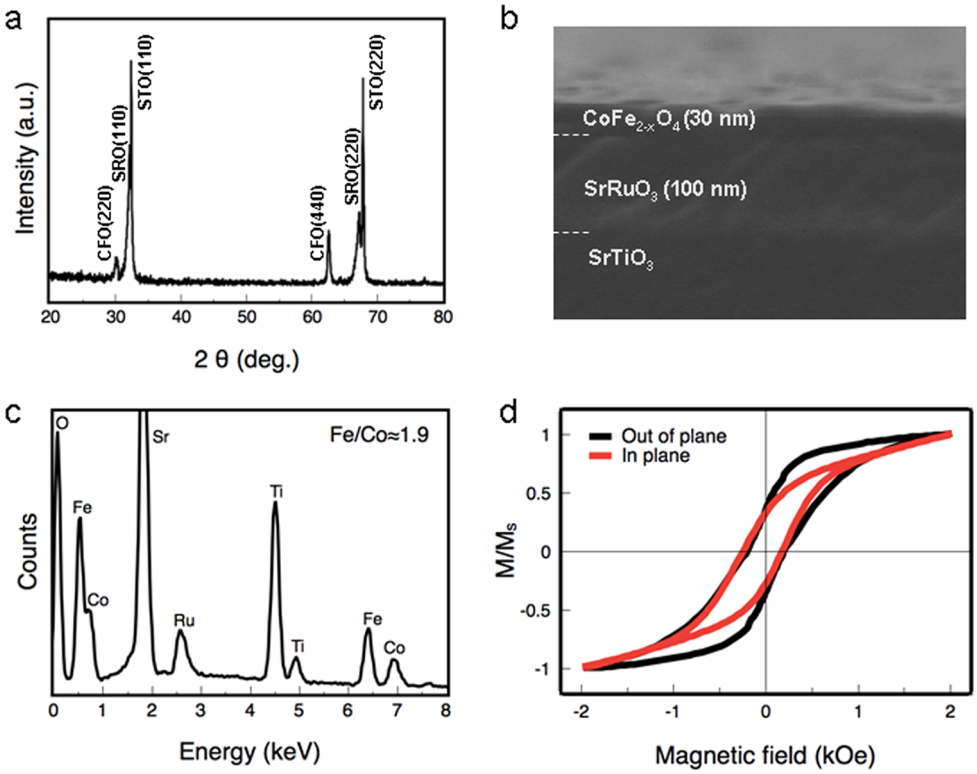

Figure 2. (a) X-ray diffractive pattern and (b) cross-sectional scanning electron microscopic image of the as-fabricated CFO/SRO/STO structure. (c) Energy-dispersive X-ray spectrum and (d) normalized in-plane and out-of-plane magnetic hysteresis loops of the as-fabricated CFO thin film.

Figure 3b, the as-fabricated CFO film has a nano-grained single-domain structure with a grain size of 60−70 nm. It is noted that a voltage of larger than ±5 V may occasionally cause electrical breakdown and morphology changes of the sample. Thus, the loaded electric bias was constrained within ±4 V throughout the present study. When a biased voltage of −3 V is applied onto the CFO film, the area of the yellow-colored region, which corresponds to the upward-oriented magnetic domains of the CFO sample with their interaction between the downward-magnetized Co/Cr-coated tip being repulsive, increases significantly (Figure 3c). On the contrary, the effect of a bias voltage of 3 V is to increase the area of the blue-colored region (Figure 3d and e), with the interaction between the magnetic tip and the downward-oriented magnetic domains being attractive. Therefore, nanoscale electric field-induced magnetization reversal can be achieved phenomenologically in the present CFO thin films at room temperature.

To confirm that the contrast change in the MFM images and thus the variation of the interaction between the SPM tip and the sample are magnetic, the magnetization of the Co/Cr-coated tip is reversed to scan the same area. For the purpose of a better illustration, zoomed-in MFM images focusing on single domains, as highlighted by the red dashed lines in Figure 4, were investigated. As shown in Figure 4a and b, the magnetization of the circled area originally oriented downward can be readily switched to be upward, upon being subjected to a biased voltage of −4 V. Once the magnetization of the Co/Cr-coated SPM tip was reversed, an almost perfect mirror image with the yellow and blue regions interchanging their color codes in good accuracy can be observed (Figure 4c). A similar phenomenon was reproduced when the sample was subjected to a biased voltage of 4 V before being scanned with a reversely magnetized SPM tip (Figure 4d, e, and f). Therefore, the influence of possible electrostatic interactions between the CFO thin film and the Co/Cr-coated magnetic tip can be excluded confidentially. On the other hand, since the average value of the current flowing through the sample is relatively small (in the range of ∼200 pA or with a current density of $\sim 10^2$ A/cm^2), the influence of a possible current-induced magnetic field or spin-torque effect on the magnetization reversal can be excluded.[1,45] Thus, the observed contrast changes induced by the applied electric fields can be readily ascribed to the switching of magnetic domains. Considering that the MFM images reflect only the domain features of CFO in the direction perpendicular to the film surface, which is also the easy axis direction of the sample, the above observation suggests that an almost 180° magnetization reversal may be realized in the present study. Nevertheless, the present electric field-induced magnetization reversal in CFO films shows a low power consumption of less than 0.1 pW,

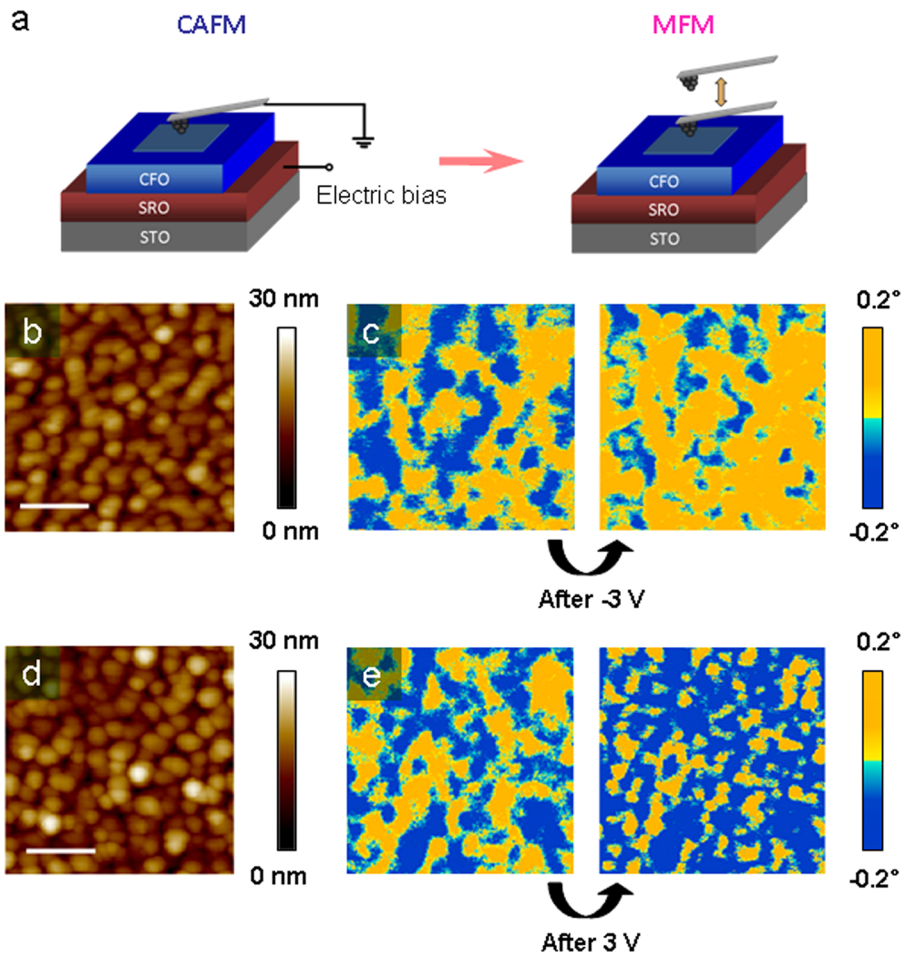

Figure 3. Electric field-induced magnetization reversal in CFO thin films. (a) Schematic illustration of the experimental setups for the C-AFM and MFM measurements. (b, d) Morphologies of the CFO thin film at the pristine state and (c, e) corresponding MFM images of the CFO thin film at the pristine state and after being subjected to biased voltages of −3 and 3 V, respectively. Scale bar: 300 nm.

as estimated with the simple equation

$$W = I^2Rt \quad (1)$$

where I is the average current value read from the C-AFM measurement (~200 pA), R is the sample resistance at −4 V (~10^{10} Ω, $R = dV/dI$), and t is the C-AFM scanning time at each pixel (~1 ms). Such a power consumption is at least 10 times smaller than that of the spin-torque devices.[46−48] However, the speed of the present ion-migration-induced magnetization reversal is probably slower than that of the magnetic read−write memories. The time required for switching the magnetization may be further decreased by increasing the amplitude of the applied voltage, according to the ion-hopping model.[49,50]

The reversibility of the magnetization reversal behavior was further assessed with the applied biased voltages running in the sequence of 0 V → −4 V → 0 V → 4 V → 0 V → −4 V (Figure 5). Initially, the magnetic domains with magnetization orienting upward and downward can be clearly differentiated in the fresh CFO sample (① of Figure 5a). After applying a negative voltage of −2 V onto the thin film, the

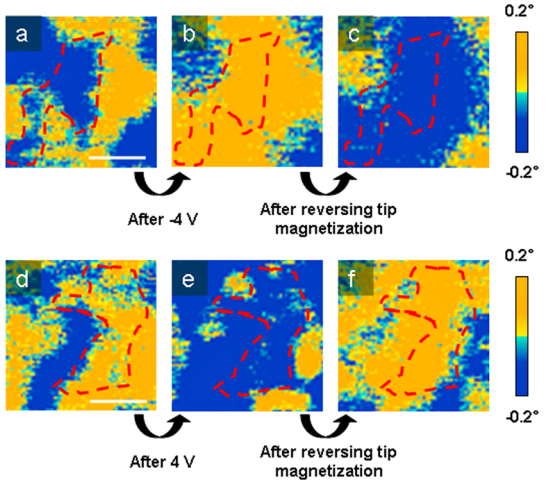

Figure 4. Verification of electric field-induced magnetization reversal by using MFM tips with opposite magnetizations. MFM images of the CFO thin film (a, d) at the pristine state, (b, e) after being subjected to biased voltages of −4 and 4 V, and (c, f) after the reversal of the magnetic tip magnetization. Scale bar: 100 nm.

yellow-colored regions with the magnetization orienting upward become larger (②). Further increasing the

magnitude of the negative voltage continuously drives the magnetization reversal, and most of the domains are switched to orienting upward with a negative voltage of −4 V (③). The magnetization of the CFO thin film does not change significantly during the negative voltage decreasing process (④), until the polarity of the external electric field is reversed. With an increase in their magnitudes, the application of positively biased voltages can switch the magnetization of the domains to orienting downward gradually and increase their spatial dimension sequentially (⑤–⑦). The reloading of the negative bias voltages then recovers the upward-oriented magnetic domain again (⑧, ⑨). By defining the contrast change ratio as that between the total areas of the electrically produced upward-magnetized domains and the initially upward-magnetized domains, up to ~70% and reversible modulation of the magnetization reversal in CFO thin films was demonstrated by the application of external electric fields (Figure 5b). When being subjected to biased voltages, the amount of migrated Co^{2+} ions can be roughly estimated by considering the probability of ion hopping to adjacent sites along the direction of the applied electric field,[49] which is proportional to $\sinh(azqE/2kT)$, where a is the hopping distance between adjacent sites, zq is the electron charges of the ion, k is the Boltzmann constant, T is temperature, and E is the electric field. For the Fe-deficient CFO film at room temperature, the

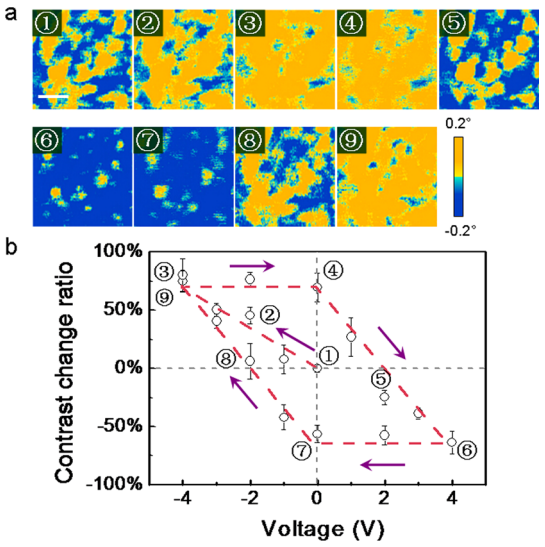

Figure 5. Reversible magnetization reversal under various electric fields. (a) MFM images of the CFO thin film at the pristine state and after being subjected to various biased voltages. Scale bar: 200 nm. (b) Evolution of the contrast change ratio after being subjected to various biased voltages in the sequence 0 V → −4 V → 0 V → 4 V → 0 V → −4 V.

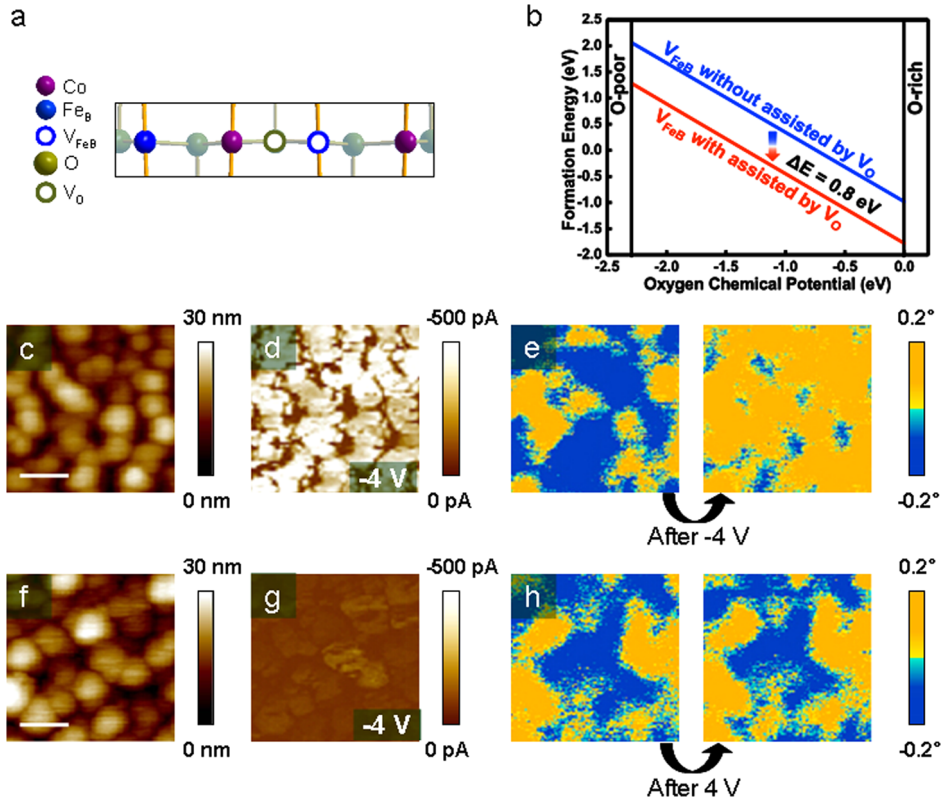

Figure 6. Oxygen pressure dependence of the magnetization reversal in CFO thin films. (a) Ground-state localized structure of the CFO thin film with a Fe vacancy and an oxygen vacancy present along the [110] direction. (b) Dependence of the formation energy of a B-site Fe vacancy on the chemical potential of oxygen, with and without the assistance of an oxygen vacancy. (c, f) Morphologies, (d, g) C-AFM images under −4 V, (e, h) MFM images at the pristine state and, after being subjected to biased voltages of −4 V, of the CFO thin films deposited under an oxygen pressure of 0.1 and 1 Pa, respectively. Scale bar: 150 nm.

hopping distance a, corresponding to the distance between the Co^{2+} ion and the adjacent cation vacancy, is calculated to be around 0.3 nm,[51] while zq is 3.2×10^{-19} C and kT is around 26 meV at room temperature. Since a biased voltage of ±4 V, which correspond an electric field of 1.33×10^8 V/m in the 30 nm CFO thin film, can reverse most of the magnetization to the opposite polarity (Figure 5a), it is reasonable to assume that the probability of Co^{2+} ion hopping into the neighboring cation vacancies under ±4 V is 100%. Similarly, the corresponding probabilities of Co^{2+} ions hopping to the neighboring cation vacancy, under ±1, ± 2, and ±3 V and with the corresponding degrees of magnetization change shown in Figure 5b, are estimated to be 17.9%, 38.6%, and 64.9%, respectively.

Calculation results also reveal that the formation energy of the B-site Fe vacancies can be further lowered when neighboring oxygen vacancies exist (Figure 6a and b). As shown in Figure 6c, d, f, and g, the CFO film deposited at a lower oxygen pressure of 0.1 Pa is more conductive than that deposited at a higher oxygen pressure of 1 Pa, which suggests that more oxygen vacancies that act as leaking sites for charge carrier transportation exist in the former sample.[52−54] The presence of a larger amount of oxygen vacancies may further facilitate the migration of the Co^{2+} ions in and promote the magnetization reversal of the CFO films under electric fields.[55−57] As a result, we observe that the magnetization modulation of the CFO film deposited at a lower oxygen pressure of 0.1 Pa (Figure 6e) is relatively easier than that of the samples fabricated at high oxygen pressures (*e.g.*, 1 Pa, Figure 6h).

CONCLUSIONS

To summarize, we have both theoretically and experimentally demonstrated that room-temperature manipulation of the nanoscale magnetization reversal can be achieved by merely applying external electric fields onto Fe-deficient cobalt ferrite thin films. The electric field-controlled magnetization reversal is nonvolatile and reversible, which can be modulated by tuning the polarity and amplitude of the applied electric fields. First-principles calculation results suggest that the observed magnetization reversal can be attributed to the reversible migration and redistribution of Co^{2+} ions between Fe vacancies and is assisted by the presence of oxygen vacancies, which in turn result in the unidirectional magnetic anisotropy of the sample along the ⟨110⟩ directions. Such a concept of modulating magnetization by nanoscale ion manipulation through electrical means is also expected to be applicable to other magnetic materials, which may help to realize the low-power spintronic devices.

METHODS

Sample Preparation. The $SrRuO_3$ thin film was deposited at a nominal temperature of 750 °C in an atmosphere of pure oxygen (10 Pa) on a commercially available $SrTiO_3$ (110) substrate with a pulsed laser deposition system. The $CoFe_{2-x}O_4$ thin film was then deposited on the $SrRuO_3$ thin film by using the pulsed laser deposition system as well. The nominal temperature of $CoFe_{2-x}O_4$ deposition is around 800 °C, while the oxygen pressure varied between 0.1 and 1 Pa. The deposition frequency of both $SrRuO_3$ and $CoFe_{2-x}O_4$ thin films was set to 2 Hz.

Measurements. The crystal structure was examined with the X-ray diffraction technique (Huber six-circle diffractometer). The magnetic hysteresis loops were obtained with a superconducting quantum interference device (Quantum Design). An atomic force microscope (Dimension V, Veeco) was used to perform both the C-AFM and MFM measurements. During the C-AFM measurement, a conducting cantilever coated with Pt/Ir (PPP-CONTPt, Nanosensors) was used in the contact mode, and the contact force was set to around 30 nN. After each C-AFM scanning operation, additional scanning processes with zero bias were performed to eliminate any possible electrostatic charges bound on the film surface. The MFM measurement was performed at a lift height of 60−80 nm with a magnetic tip coated with a Co/Cr thin film (MESP, Bruker). Before MFM measurements, a magnetic field of around 2000 Oe was employed to initialize the magnetization of the magnetic tip to the upward or downward orientation. During the measurements, the tips were always grounded to minimize the noise.

First-Principles Calculation and Modeling. First-principles calculation was performed based on density functional theory (DFT) using the Vienna ab initio simulation package (VASP).[58] Projector augmented wave (PAW) potentials were employed to model the electron−ion interaction.[59] Generalized gradient approximation (GGA)[60] with Perdew−Burke−Ernzerhof (PBE)[61] functions was used to approximate exchange and correlation effects for structural relaxation. The cutoff energy for the plane-wave basis restriction was set at 400 eV in all calculations. K-points for the Brillouin-zone integration were sampled under Monkhorst−Pack.[62] The structures were fully relaxed until the forces acting on all atoms were less than 0.02 eV/Å and the self-consistency accuracy for electronic loops reached 10^{-4} eV. Our simulated lattice parameters of an unstrained bulk Co-ferrite unit cell are $a = b = c = 8.349$ Å. The formation energies of ion vacancies were calculated in a neutral state with the following equation: $E_f^{Vac} = E_{tot}^{Vac} - E_{tot}^{0} + E_{atom}^{Vac}$, where E_{tot}^{Vac} is the total energy of the unit cell with vacancy defect ($V_{ac} = V_O$, V_{Co}, V_{FeA}, or V_{FeB}), E_{tot}^{0} is the total energy of the perfect Co-ferrite unit cell, and E_{atom}^{Vac} is the energy of the corresponding isolated vacancy atom (O, Co, Fe_A, or Fe_B) in a vacuum. The migration barriers for defects motion in Co-ferrite were calculated by the nudged elastic band method (NEB) of the VTST code as implanted in VASP.[63,64] The images of NEB were relaxed until the maximum residual force was less than 0.02 eV/Å. Uniaxial magnetic anisotropy along the [110] and [$\bar{1}\bar{1}$0] directions was simulated by noncollinear calculations, which were performed by considering spin−orbital coupling using the algorithm implanted in VASP by Hobbs *et al.*[65]

Conflict of Interest: The authors declare no competing financial interest.

Acknowledgment. The authors acknowledge the financial support from the State Key Project of Fundamental Research of China (973 Program, 2012CB933004), National Natural Science Foundation of China (11274321, 11474295, 51303194, 61328402), the Instrument Developing Project of the Chinese Academy of Sciences (YZ201327), the Youth Innovation Promotion Association of the Chinese Academy of Sciences, Ningbo Natural Science Foundations (2013A610031), and Ningbo International Cooperation Projects (2012D10018, 2014D10005).

REFERENCES AND NOTES

1. Chappert, C.; Fert, A.; Van Dau, F. N. The Emergence of Spin Electronics in Data Storage. *Nat. Mater.* **2007**, *6*, 813–823.
2. Mangin, S.; Ravelosona, D.; Katine, J. A.; Carey, M. J.; Terris, B. D.; Fullerton, E. E. Current-Induced Magnetization Reversal in Nanopillars with Perpendicular Anisotropy. *Nat. Mater.* **2006**, *5*, 210–215.
3. Cherifi, R. O.; Ivanovskaya, V.; Phillips, L. C.; Zobelli, A.; Infante, I. C.; Jacquet, E.; Garcia, V.; Fusil, S.; Briddon, P. R.; Guiblin, N. M.; *et al.* Electric-Field Control of Magnetic Order above Room Temperature. *Nat. Mater.* **2014**, *13*, 345–351.
4. Zavaliche, F.; Zheng, H.; Mohaddes-Ardabili, L.; Yang, S. Y.; Zhan, Q.; Shafer, P.; Reilly, E.; Chopdekar, R.; Jia, Y.; Wright, P.; *et al.* Electric Field-Induced Magnetization Switching in Epitaxial Columnar Nanostructures. *Nano Lett.* **2005**, *5*, 1793–1796.
5. Zavaliche, F.; Zhao, T.; Zheng, H.; Straub, F.; Cruz, M. P.; Yang, P. L.; Hao, D.; Ramesh, R. Electrically Assisted Magnetic Recording in Multiferroic Nanostructures. *Nano Lett.* **2007**, *7*, 1586–1590.
6. Ostler, T. A.; Barker, J.; Evans, R. F. L.; Chantrell, R. W.; Atxitia, U.; Chubykalo-Fesenko, O.; El Moussaoui, S.; Le Guyader, L.; Mengotti, E.; Heyderman, L. J.; *et al.* Ultrafast Heating as a Sufficient Stimulus for Magnetization Reversal in a Ferrimagnet. *Nat. Commun.* **2012**, *3*, 666.
7. Ramesh, R.; Spaldin, N. A. Multiferroics: Progress and Prospects in Thin Films. *Nat. Mater.* **2007**, *6*, 21–29.
8. Wang, Y.; Hu, J.; Lin, Y.; Nan, C.-W. Multiferroic Magnetoelectric Composite Nanostructures. *NPG Asia Mater.* **2010**, *2*, 61–68.
9. Hur, N.; Park, S.; Sharma, P. A.; Ahn, J. S.; Guha, S.; Cheong, S. W. Electric Polarization Reversal and Memory in a Multiferroic Material Induced by Magnetic Fields. *Nature* **2004**, *429*, 392–395.
10. Radaelli, G.; Petti, D.; Plekhanov, E.; Fina, I.; Torelli, P.; Salles, B. R.; Cantoni, M.; Rinaldi, C.; Gutierrez, D.; Panaccione, G.; *et al.* Electric Control of Magnetism at the Fe/$BaTiO_3$ Interface. *Nat. Commun.* **2014**, *5*, 4404.
11. Zhang, S.; Zhao, Y. G.; Xiao, X.; Wu, Y. Z.; Rizwan, S.; Yang, L. F.; Li, P. S.; Wang, J. W.; Zhu, M. H.; Zhang, H. Y.; *et al.* Giant Electrical Modulation of Magnetization in $Co_{40}Fe_{40}B_{20}$/$Pb(Mg_{1/3}Nb_{2/3})_{0.7}Ti_{0.3}O_3$(011) Heterostructure. *Sci. Rep.* **2013**, *4*, 3727.
12. Skumryev, V.; Laukhin, V.; Fina, I.; Marti, X.; Sanchez, F.; Gospodinov, M.; Fontcuberta, J. Magnetization Reversal by Electric-Field Decoupling of Magnetic and Ferroelectric Domain Walls in Multiferroic-Based Heterostructures. *Phys. Rev. Lett.* **2011**, *106*, 057206.
13. Chiba, D.; Yamanouchi, M.; Matsukura, F.; Ohno, H. Electrical Manipulation of Magnetization Reversal in a Ferromagnetic Semiconductor. *Science* **2003**, *301*, 943–945.
14. Yamada, Y.; Ueno, K.; Fukumura, T.; Yuan, H. T.; Shimotani, H.; Iwasa, Y.; Gu, L.; Tsukimoto, S.; Ikuhara, Y.; Kawasaki, M. Electrically Induced Ferromagnetism at Room Temperature in Cobalt-Doped Titanium Dioxide. *Science* **2011**, *332*, 1065–1067.
15. Maruyama, T.; Shiota, Y.; Nozaki, T.; Ohta, K.; Toda, N.; Mizuguchi, M.; Tulapurkar, A. A.; Shinjo, T.; Shiraishi, M.; Mizukami, S.; *et al.* Large Voltage-Induced Magnetic Anisotropy Change in a Few Atomic Layers of Iron. *Nat. Nanotechnol.* **2009**, *4*, 158–161.
16. Ghidini, M.; Pellicelli, R.; Prieto, J. L.; Moya, X.; Soussi, J.; Briscoe, J.; Dunn, S.; Mathur, N. D. Non-Volatile Electrically-Driven Repeatable Magnetization Reversal with No Applied Magnetic Field. *Nat. Commun.* **2013**, *4*, 1453.
17. Chai, Y. S.; Kwon, S.; Chun, S. H.; Kim, I.; Jeon, B. G.; Kim, K. H.; Lee, S. Electrical Control of Large Magnetization Reversal in a Helimagnet. *Nat. Commun.* **2014**, *5*, 4208.
18. Cuellar, F. A.; Liu, Y. H.; Salafranca, J.; Nemes, N.; Iborra, E.; Sanchez-Santolino, G.; Varela, M.; Hernandez, M. G.; Freeland, J. W.; Zhernenkov, M.; *et al.* Reversible Electric-Field Control of Magnetization at Oxide Interfaces. *Nat. Commun.* **2014**, *5*, 5215.
19. Li, P. S.; Chen, A. T.; Li, D. L.; Zhao, Y. G.; Zhang, S.; Yang, L. F.; Liu, Y.; Zhu, M. H.; Zhang, H. Y.; Han, X. F. Electric Field Manipulation of Magnetization Rotation and Tunneling Magnetoresistance of Magnetic Tunnel Junctions at Room Temperature. *Adv. Mater.* **2014**, *26*, 4320–4325.
20. Waser, R.; Aono, M. Nanoionics-Based Resistive Switching Memories. *Nat. Mater.* **2007**, *6*, 833–840.
21. Wang, Y. C.; Ou, J. Z.; Balendhran, S.; Chrimes, A. F.; Mortazavi, M.; Yao, D. D.; Field, M. R.; Latham, K.; Bansal, V.; Friend, J. R.; *et al.* Electrochemical Control of Photoluminescence in Two-Dimensional MoS_2 Nanoflakes. *ACS Nano* **2013**, *7*, 10083–10093.
22. Hu, B. L.; Zhu, X. J.; Chen, X. X.; Pan, L.; Peng, S. S.; Wu, Y. Z.; Shang, J.; Liu, G.; Yan, Q.; Li, R.-W. A Multilevel Memory Based on Proton-Doped Polyazomethine with an Excellent Uniformity in Resistive Switching. *J. Am. Chem. Soc.* **2012**, *134*, 17408–17411.
23. He, C. L.; Li, J. F.; Wu, X.; Chen, P.; Zhao, J.; Yin, K. B.; Cheng, M.; Yang, W.; Xie, G. B.; Wang, D. M.; *et al.* Tunable Electroluminescence in Planar Graphene/SiO_2 Memristors. *Adv. Mater.* **2013**, *25*, 5593–5598.
24. Shang, J.; Liu, G.; Yang, H. L.; Zhu, X. J.; Chen, X. X.; Tan, H. W.; Hu, B. L.; Pan, L.; Xue, W. H.; Li, R.-W. Thermally Stable Transparent Resistive Random Access Memory Based on All-Oxide Heterostructures. *Adv. Funct. Mater.* **2014**, *24*, 2171–2179.
25. Xue, W. H.; Xiao, W.; Chen, X. X.; Zhu, X. J.; Shang, J.; Pan, L.; Tan, H. W.; Liu, G.; Xu, X. H.; Ding, J.; *et al.* Intrinsic and Interfacial Effect of Electrode Metals on the Resistive Switching Behaviors of Zinc Oxide Films. *Nanotechnology* **2014**, *25*, 425204.
26. Pan, L.; Liu, G.; Li, H.; Meng, S.; Han, L.; Chen, B.; Shang, J.; Prats, A. E. P.; Lu, W.; Zou, X. D.; Li, R.-W. A Resistance-Switchable and Ferroelectric Metal−Organic Framework. *J. Am. Chem. Soc.* **2014**, *136*, 17477–17483.
27. Dasgupta, S.; Das, B.; Knapp, M.; Brand, R. A.; Ehrenberg, H.; Kruk, R.; Hahn, H. Intercalation-Driven Reversible Control of Magnetism in Bulk Ferromagnets. *Adv. Mater.* **2014**, *26*, 4639–4644.
28. Bauer, U.; Yao, L.; Tan, A. J.; Agrawa, P.; Emori, S.; Tuller, H. L.; Dijken, S.; Beach, G. S. D. Magneto-Ionic Control of Interfacial Magnetism. *Nat. Mater.* **2015**, *14*, 174–181.
29. Zhu, X.-J.; Shang, J.; Liu, G.; Li, R.-W. Ion Transport Related Resistive Switching in Film Sandwich Structures. *Chin. Sci. Bull.* **2014**, *59*, 2363–2382.
30. Grigorova, M.; Blythe, H. J.; Blaskov, V.; Rusanov, V.; Petkov, V.; Masheva, V.; Nihtianova, D.; Martinez, L. M.; Munoz, J. S.; Mikhov, M. Magnetic Properties and Mössbauer Spectra of Nanosized $CoFe_2O_4$ Powders. *J. Magn. Magn. Mater.* **1998**, *183*, 163–172.
31. Zhang, Z. T.; Rondinone, A. J.; Ma, J. X.; Shen, J.; Dai, S. Morphologically Templated Growth of Aligned Spinel $CoFe_2O_4$ Nanorods. *Adv. Mater.* **2005**, *17*, 1415–1419.
32. Fritsch, D.; Ederer, C. Effect of Epitaxial Strain on the Cation Distribution in Spinel Ferrites $CoFe_2O_4$ and $NiFe_2O_4$: A Density Functional Theory Study. *Appl. Phys. Lett.* **2011**, *99*, 081916.
33. Tachiki, M. Origin of the Magnetic Anisotropy Energy of Cobalt Ferrite. *Prog. Theor. Phys.* **1960**, *23*, 1055–1072.
34. Iida, S. The Role of Cation Vacancy in Magnetic Annealing of Iron-Cobalt Ferrites. *J. Appl. Phys.* **1960**, *31*, S251–S258.
35. Iida, S.; Miwa, H. Theory of the Relaxation of the Uniaxial Anisotropy Induced by Ionic Migration in Iron-Cobalt Ferrites. *J. Phys. Soc. Jpn.* **1966**, *21*, 2505–2539.
36. Bickford, L. R.; Brownlow, J. M.; Penoyer, R. F. Effect of Cation Vacancies on the Magnetic Annealing of Cobalt-Substituted Magnetite. *J. Appl. Phys.* **1958**, *29*, 441–442.
37. Prince, E. Neutron Diffraction Observation of Heat Treatment in Cobalt Ferrite. *Phys. Rev.* **1956**, *102*, 674–676.
38. Na, J. G. Mössbauer Effect Study of the Relaxation Phenomenon of Cobalt Ferrite Thin Films. *J. Mater. Sci. Lett.* **1998**, *17*, 229–231.
39. Zhu, X. J.; Ong, C. S.; Xu, X. X.; Hu, B. L.; Shang, J.; Yang, H. L.; Katlakunta, S.; Liu, Y. W.; Chen, X. X.; Pan, L.; *et al.* Direct Observation of Lithium-Ion Transport under an Electrical Field in Li_xCoO_2 Nanograins. *Sci. Rep.* **2013**, *3*, 1084.

40. Liu, Q.; Sun, J.; Lv, H. B.; Long, S. B.; Yin, K. B.; Wan, N.; Li, Y. T.; Sun, L. T.; Liu, M. Real-Time Observation on Dynamic Growth/Dissolution of Conductive Filaments in Oxide-Electrolyte-Based ReRAM. *Adv. Mater.* **2012**, *24*, 1844–1849.
41. Yang, Y. C.; Gao, P.; Gaba, S.; Chang, T.; Pan, X. Q.; Lu, W. Observation of Conducting Filament Growth in Nanoscale Resistive Memories. *Nat. Commun.* **2012**, *3*, 732.
42. Chinnasamy, C. N.; Jeyadevan, B.; Shinoda, K.; Tohji, K.; Djayaprawira, D. J.; Takahashi, M.; Joseyphus, R. J.; Narayanasamy, A. Unusually High Coercivity and Critical Single-Domain Size of Nearly Monodispersed $CoFe_2O_4$ Nanoparticles. *Appl. Phys. Lett.* **2003**, *83*, 2862–2864.
43. Ranvah, N.; Melikhov, Y.; Jiles, D. C.; Snyder, J. E.; Moses, A. J.; Williams, P. I.; Song, S. H. Temperature Dependence of Magnetic Anisotropy of Ga-Substituted Cobalt Ferrite. *J. Appl. Phys.* **2008**, *103*, 07E506.
44. Wang, Z.; Li, Y.; Viswan, R.; Hu, B.; Harris, V. G.; Li, J.; Viehland, D. Engineered Magnetic Shape Anisotropy in $BiFeO_3$-$CoFe_2O_4$ Self-Assembled Thin Films. *ACS Nano* **2013**, *7*, 3447–3456.
45. Gambardella, P.; Miron, I. M. Current-Induced Spin-Orbit Torques. *Philos. Trans. R. Soc. A* **2011**, *369*, 3175–3197.
46. Slonczewski, J. C. Current-Driven Excitation of Magnetic Multilayers. *J. Magnetism Magn. Mater.* **1996**, *159*, L1–L7.
47. Radaelli, G.; Petti, D.; Plekhanov, E.; Fina, I.; Torelli, P.; Salles, B. R.; Cantoni, M.; Rinaldi, C.; Gutiérrez, D.; Panaccione, G.; *et al.* Electric Control of Magnetism at the Fe/$BaTiO_3$ Interface. *Nat. Commun.* **2014**, *5*, 3404.
48. Zhang, L.; Zhao, W.; Zhuang, Q.; Bao, J.; Wang, G.; Tang, H.; Li, C.; Xu, B. A 16 Kb Spin-Transfer Torque Random Access Memory with Self-Enable Switching and Precharge Sensing Schemes. *IEEE Trans. Magn.* **2014**, *50*, 3400107.
49. Waser, R.; Dittmann, R.; Staikov, G.; Szot, K. Redox-Based Resistive Switching Memories - Nanoionic Mechanisms, Prospects, and Challenges. *Adv. Mater.* **2009**, *21*, 2632–2663.
50. Jo, S. H.; Kim, K.-H.; Lu, W. Programmable Resistance Switching in Nanoscale Two-Terminal Devices. *Nano Lett.* **2009**, *9*, 496–500.
51. Hou, Y. H.; Zhao, Y. J.; Liu, Z. W.; Yu, H. Y.; Zhong, X. C.; Qiu, w. Q.; Zeng, D. C.; Wen, L. S. Structural, Electronic and Magnetic Properties of Partially Inverse Spinel $CoFe_2O_4$: A First-Principles Study. *J. Phys. D: Appl. Phys.* **2010**, *43*, 445003.
52. Park, J.-W.; Park, J.-W.; Jung, K.; Yang, M. K.; Lee, J.-K. Influence of Oxygen Content on Electrical Properties of NiO Films Grown by RF Reactive Sputtering for Resistive Random-Access Memory Applications. *J. Vac. Sci. Technol. B* **2006**, *24*, 2205–2208.
53. Park, S.-G.; Magyari-Kope, B.; Nishi, Y. Impact of Oxygen Vacancy Ordering on the Formation of a Donductive Filament in TiO_2 for Resistive Switching Memory. *IEEE Electron Device Lett.* **2011**, *32*, 197–199.
54. Szot, K.; Speier, W.; Bihlmayer, G.; Waser, R. Switching the Electrical Resistance of Individual Dislocations in Single-Crystalline $SrTiO_3$. *Nat. Mater.* **2006**, *5*, 312–320.
55. Ayyappan, S.; Raja, S. P.; Venkateswaran, C.; Philip, J.; Raj, B. Room Temperature Ferromagnetism in Vacuum Annealed Nanoparticles. *Appl. Phys. Lett.* **2010**, *96*, 143106.
56. Jaffari, G. H.; Rumaiz, A. K.; Woicik, J. C.; Shah, S. I. Influence of Oxygen Vacancies on the Electronic Structure and Magnetic Properties of $NiFe_2O_4$ Thin Films. *J. Appl. Phys.* **2012**, *111*, 093906.
57. Anjum, S.; Jaffari, G. H.; Abdul, K. R.; Rafique, M. S.; Shah, S. I. Role of Vacancies in Transport and Magnetic Properties of Nickel Ferrite Thin Films. *J. Phys. D: Appl. Phys.* **2010**, *43*, 265001.
58. Kresse, G.; Furthmüller, J. Efficient Iterative Schemes for ab Initio Total-Energy Calculations Using a Plane-Wave Basis Set. *Phys. Rev. B* **1996**, *54*, 11169–11186.
59. Blöchl, P. E. Projector Augmented-Wave Method. *Phys. Rev. B* **1994**, *50*, 17953–17979.
60. Perdew, J. P.; Chevary, J. A.; Vosko, S. H.; Jackson, K. A.; Pederson, M. R.; Singh, D. J.; Fiolhais, C. Atoms, Molecules, Solids, and Surfaces: Applications of the Generalized Gradient Approximation for Exchange and Correlation. *Phys. Rev. B: Condens Matter* **1992**, *46*, 6671–6687.
61. Perdew, J. P.; Burke, K.; Ernzerhof, M. Generalized Gradient Approximation Made Simple. *Phys. Rev. Lett.* **1996**, *77*, 3865–3868.
62. Monkhorst, H. J.; Pack, J. D. Special Points for Brillouin-Zone Integrations. *Phys. Rev. B* **1976**, *13*, 5188–5192.
63. Henkelman, G.; Jóhannesson, G.; Jónsson, H. Methods for Finding Saddle Points and Minimum Energy Caths. In *Theoretical Methods in Condensed Phase Chemistry*; Schwartz, S. D., Ed.; Springer: The Netherlands, 2002; pp 269−302.
64. Henkelman, G.; Uberuaga, B. P.; Jónsson, H. A Climbing Image Nudged Elastic Band Method for Finding Saddle Points and Minimum Energy Paths. *J. Chem. Phys.* **2000**, *113*, 9901–9904.
65. Hobbs, D.; Kresse, G.; Hafner, J. Fully Unconstrained Noncollinear Magnetism within the Projector Augmented-Wave Method. *Phys. Rev. B* **2000**, *62*, 11556–11570.